# Influence of the solar wind dynamic pressure on the decay and injection of the ring current

C. B. Wang[1] and J. K. Chao
Institute of Space Science, National Central University, Jung-li, Taiwan

C.-H. Lin
Department of Electrical Engineering, Ching-Yun Institute of Technology, Jung-li, Taiwan

Received 19 January 2003; revised 6 May 2003; accepted 3 June 2003; published 11 September 2003.

[1] The influence of the solar wind dynamic pressure on the decay and injection of the ring current is investigated empirically, on the basis of the solar wind and the geomagnetic index *Dst* of the OMNI database, for the period from January 1964 to July 2001. We found that when the position of the ring current is closer to the Earth for a higher solar wind dynamic pressure, the decay time of the ring current decreases. The decay time, in hours, varies as follows, $\tau = 8.70 \exp(6.66/(6.04 + P))$, for northward interplanetary magnetic fields (IMF), where $P$ is the solar wind dynamic pressure in nanopascals. It is also found, by minimizing the root mean square errors of the hourly *Dst* difference between the calculated values and the measured ones, that the ring current injection rate is proportional to the solar wind dynamic pressure, with a power index equal to 0.2 during southward IMF. This implies that the ring current injection increases when the magnetosphere is more compressed by high solar wind dynamic pressure. On the basis of our new results we demonstrate that the predictions of *Dst* using *O'Brien and McPherron*'s [2000a] model are improved, especially for intense geomagnetic storms when the influence of the solar wind dynamic pressure on the decay and injection of ring current is taken into consideration. *INDEX TERMS:* 2778 Magnetospheric Physics: Ring current; 2788 Magnetospheric Physics: Storms and substorms; 2722 Magnetospheric Physics: Forecasting; 2784 Magnetospheric Physics: Solar wind/magnetosphere interactions; *KEYWORDS:* ring current, *Dst* index, forecasting, storms and substorms, solar wind/magnetospheric interactions

**Citation:** Wang, C. B., J. K. Chao, and C.-H. Lin, Influence of the solar wind dynamic pressure on the decay and injection of the ring current, *J. Geophys. Res.*, *108*(A9), 1341, doi:10.1029/2003JA009851, 2003.

## 1. Introduction

[2] When the interplanetary magnetic field (IMF) reaches the Earth with a southward orientation, magnetic reconnection between the Earth's magnetic field and IMF will take place. As a result, the Earth's magnetic field will be able to connect to the IMF directly, so that energetic particles in the solar wind are free to enter the magnetosphere along the magnetic field lines. If this process continues for several hours, the magnetic field, as well as plasma in the magnetosphere, will be strongly disturbed by the solar wind, and a geomagnetic storm or substorm will develop [*Gonzalez et al.*, 1994]. Geomagnetic storms are characterized by a depression in the $H$ component of the geomagnetic field lasting over some tens of hours. This depression is mainly caused by the ring current encircling the Earth in a westward direction and can be monitored by the *Dst* index [*Kamide et al.*, 1998; *Daglis et al.*, 1999].

[3] The *Dst* index can be calculated by measuring the horizontal geomagnetic field component at four low-latitude ground observatories, which represents the effects of several current systems on the low-latitude geomagnetic field [*Akasofu and Chapman*, 1972; *Campbell*, 1996; *Rostoker et al.*, 1997]. Numerous studies have been published on the relative contributions of different terrestrial and magnetospheric currents to the *Dst* index. It is found that the magnetotail currents, the substorm current wedges and the Earth-induced currents in the ground can produce significant perturbations on the Earth's surface field such as the *Dst* index during the periods of high magnetospheric activity [e.g., *Langel and Estes*, 1985; *Alexeev et al.*, 1996; *Friedrich et al.*, 1999; *Turner et al.*, 2000; *Häkkinen et al.*, 2002]. In general, it is believed that the ring current gives the main contribution to the *Dst* index [e.g., *Hamilton et al.*, 1988; *Roeder et al.*, 1996; *Jordanova et al.*, 1998; *Greenspan and Hamilton*, 2000], and the ring current may be spatially asymmetric in the main phase of a storm [e.g., *Akasofu and Chapman*, 1972]. Variations of the *Dst* index can be interpreted as a measurement of the kinetic energy of

[1] Also at School of Earth and Space Sciences, University of Science and Technology of China, Anhui, China.


0148-0227/03/2003JA009851$09.00

the particles that make up the ring current, which is given by the following equation [*Dessler and Parker*, 1959; *Sckopke*, 1966]:

$$\frac{Dst^*(t)}{B_0} = \frac{2E(t)}{3E_m}. \quad (1)$$

Here $B_0$ and $E_m$ are the magnetic field at the surface of the Earth and the total magnetic energy of the geomagnetic field above the Earth's surface, respectively, while $E(t)$ is the total kinetic energy of the charge particles in the ring current at time $t$ and $Dst^*$ is simply the pressure-corrected $Dst$, from which the contribution of the magnetopause current to $Dst$ has been eliminated by the following equation:

$$Dst^* = Dst - b\sqrt{P} + c. \quad (2)$$

Here $P$ is the solar wind dynamic pressure, $b$ is a constant of proportionality, relating changes in the $Dst$ to changes in the pressure, and $c$ is a constant representing the effects of both the quiet time magnetopause and the ring currents. The temporal variation of $E(t)$ can be simply assumed to be a combination of a source $U$ and a loss term with a simple decay time $\tau$ as follows:

$$\frac{d}{dt}E(t) = U(t) - \frac{E(t)}{\tau}. \quad (3)$$

Since $B_0$ and $E_m$ can be considered as constant, the Burton equation is obtained by substituting equation (1) into equation (3) [*Burton et al.*, 1975]

$$\frac{d}{dt}Dst^*(t) = Q(t) - \frac{Dst^*(t)}{\tau}. \quad (4)$$

Here $\tau$ and $Q(=2B_0U/3E_m)$ are the decay time and the injection term of the ring current, respectively. The magnetospheric ring current injection and decay processes have been studied in numerous works [e.g., *Tsurutani et al.*, 1985; *Feldstein*, 1992, and references therein; *Fenrich and Luhmann*, 1998; *O'Brien and McPherron*, 2000a; *McPherron and O'Brien*, 2001; *Dasso et al.*, 2002].

[4] The value of $\tau$ depends essentially on the geocentric distance, the ion composition, and the ion energy of the ring current. Numerous studies on the ring current decay time are based on ground-based geomagnetic field data obtained during magnetic storms [*Feldstein*, 1992, and references therein]. It has been found that $\tau$ changes substantially during the main and recovery phases of a magnetic storm. During the main phase of a storm, the value of $\tau$ decreases as the ring current injection increases. The most recent statistical work of *Dasso et al.* [2002] shows that the decay time spans from ~6 to 23 hours, with a mean value of $\tau$ = 14 ± 4 hours in the recovery phases for 300 intense magnetic storms that occurred from 1 January 1957 to 31 December 1998. The decay time also does not seem to remain constant over time as the recovery phase progresses. For intense storms, $\tau$ decreases as the strength of the storm increases.

[5] The ring current ions may be lost due to several physical processes such as the charge exchange with neutral atoms, the Coulomb collisions, the wave-particle interactions, and the drifting lost from the dayside magnetopause [e.g., *Fok et al.*, 1991, 1995; *Jordanova et al.*, 1996; *Daglis et al.*, 1999; *Liemohn et al.*, 1999, 2001]. It is generally believed that the main mechanism for the decay of the ring current is the charge exchange between the ring current ions and the geocorona neutral atoms [*Daglis et al.*, 1999]. On the other hand, *Fok et al.* [1991] found that Coulomb lifetimes for heavy ring current ions can be comparable to charge exchange lifetimes at energies near the peak of the ring current differential number density. For intense-to-great geomagnetic storms, the timescales of the ring current energy loss during the main phases may reach values as low as 0.5–1.0 hours, far too rapid from charge exchange or Coulomb collision processes [*Gonzalez et al.*, 1989; *Prigancová and Feldstein*, 1992]. This may be due to the scattering of ring current ions by electromagnetic ion cyclotron waves [*Jordanova et al.*, 1996]. *Liemohn et al.* [1999, 2001] suggest that losses from flow-out of the dayside magnetopause can be the dominant ring current decay term during the early part of the recovery phase. The lifetime of ring current is also dependent on ring current ion composition. Ion composition observation on the ring current shows that $O^+$ contributes substantially to the ring current, which becomes increasingly important with geomagnetic activity, and eventually dominates the ring current during great storms [*Hamilton et al.*, 1988; *Daglis et al.*, 1993; *Daglis*, 1997]. These $O^+$ ions are injected from the ionosphere to magnetosphere and subsequently convected to the ring current belt during successive intense substorms [*Daglis and Axford*, 1996]. A large $O^+$ component will induce a fast initial ring current decay, just after the storm maximum, due to the rapid loss of high-energy $O^+$ [*Smith et al.*, 1981; *Daglis*, 1997]. A detailed investigation on the relative importance of these different processes on the ring current decay is beyond the scope of this paper. We simply suppose that the effective ring current decay time is related to the mean charge exchange lifetime of energetic ions confined to the equatorial plane. Then, the decay time can be written as

$$\tau = [n(r)\sigma v]^{-1} \cos^{\gamma_m} \lambda_m, \quad (5)$$

where $n(r)$ is the neutral hydrogen density in the equatorial plane (which depends on the distance from the Earth, $r$), $\sigma$ is the cross section for the ion charge exchange, $v$ is the effective velocity of the ions, and $\lambda_m$ is the effective mirror latitude of the ions mirroring off the geomagnetic equator. *Smith and Bewtra* [1978] and *Cowley* [1977] independently found that for typical ring current altitudes, $\gamma_m \approx 3$–4. The neutral hydrogen density decreases exponentially with the distance from the Earth as

$$n(r) \propto e^{-r/r_0}. \quad (6)$$

Here $r_0$ is the scale height. One can see from equations (5) and (6) that the decay time of the ring current is strongly dependent on its distance from the Earth. Using a physical analysis of the convection pattern of the hot ions that make up the ring current, *O'Brien and McPherron* [2000a] made the assumption that the position of the ring current is

controlled by the interplanetary electrical field $VB_s$ during the ring current injection period for a southward IMF. They found that the decay time in hours varies as

$$\tau = 2.40e^{9.74/(4.69+VB_s)}, \quad (7)$$

where $VB_s$ is in mV m$^{-1}$. Here $VB_s$ is defined by

$$VB_s = \begin{cases} |VB_z| & B_z < 0 \\ 0 & B_z \geq 0 \end{cases}, \quad (8)$$

where $V$ is the bulk speed of the solar wind and $B_z$ is the $z$ component of the IMF in the Geocentric Solar Magnetospheric coordinate system. For a northward IMF, namely a positive $B_z$, there will be no significant convection in the magnetosphere, and $VB_s = 0$ is assumed. However, in this study we postulate that the position of the ring current is controlled by the size of the magnetosphere or the solar wind dynamic pressure when the IMF is northward; hence the decay time $\tau$ should be a function of $P$ or the size of the magnetosphere. This will be investigated in detail in section 2.

[6] An important step in modeling the injection function $Q$ of the ring current from the solar wind parameters was made by *Burton et al.* [1975], who related $Q$ in a simple linear way to the solar wind electric field $VB_s$. Plasma is injected into the ring current only under the influence of a southward IMF component, and the dawn-dusk electric field component in the interplanetary medium is below 0.5 mV m$^{-1}$. Recently, *O'Brien and McPherron* [2000a] verified these results from an empirical phase space analysis of the ring current dynamics. On the other hand, *Perreault and Akasofu* [1978] and *Akasofu* [1981] considered that the injection into the ring current would occur not only in the southward IMF interval but also for a northward IMF; thus $Q$ would depend on the solar wind-magnetosphere energy coupling parameter, $\varepsilon = VB^2 \sin^4(\phi/2)$, where $B$ and $\phi$ are the strength and the clock angle of the IMF, respectively. In this study, we use only the solar wind electric field $VB_s$ to model the injection function, similar to the method of *O'Brien and McPherron* [2000a].

[7] Does the solar wind density or the solar wind dynamic pressure play a role in the injection of the ring current? *Murayama* [1982] tried to model the ring current using the injection functions $Q \sim VB_s$, $Q \sim V^2B_s$, $Q \sim \varepsilon$, and $Q \sim VB_sP^{1/3}$ and found that the function $Q \sim VB_sP^{1/3}$ fits the data the best. In addition, an optimized coupling function, given by $Q \sim B_s^{1.09}V^{2.06}N^{0.39}$ where $N$ is the solar wind proton density, was used by *Murayama* [1986] and *Maezawa and Murayama* [1986]. *Fenrich and Luhmann* [1998] also considered that the ring current injection rate would increase during a period of enhanced solar wind dynamic pressure and modified the Burton equation's injection formula by $Q \sim (VB_s - 0.5)P^{1/3}$. Recently, *O'Brien and McPherron* [2000b] implemented three models for predicting the evolution of the ring current index *Dst* in real time. The three models were, *O'Brien and McPherron*'s model [2000a], *Fenrich and Luhmann*'s [1998] model, and *Burton et al.*'s [1975] model. The coefficients of the latter have been recalculated based on the 1964–1996 OMNI data set. The results, based on a period from 14 May to 31 December 1998, show that the model of *O'Brien and McPherron* [2000a], which does not include the influence of the solar wind dynamic pressure on the ring current injection, achieves the best predictions among the three models. All the above studies and comparisons are based on small and/or different data sets. It is difficult to draw meaningful inferences from a direct comparison of these works. In our investigations, based on the most recent OMNI data set, from 1964 to 2001, we find that the solar wind dynamic pressure does play an essential role in controlling the injection of the ring current, especially during strong magnetic storms.

[8] This paper presents an empirical model for the decay and injection of the ring current, which adds the influence of solar wind dynamic pressure to the decay and injection functions. The investigation of the influences on the decay time and the ring current injection, using the OMNI database, is discussed in sections 2 and 3, respectively. In section 4 the new relationship is applied to *Dst* prediction. In section 5 a discussion of the result is given. Finally, the main results are summarized in section 6.

## 2. Dependence of the Decay Time on Solar Wind Dynamic Pressure

[9] The interplanetary data and the geomagnetic indices *Dst* for this paper were obtained from the OMNI database of the National Space Science Data Center (available at ftp://nssdcftp.gsfc.nasa.gov/spacecraft_data/omni). The OMNI database includes a compilation of the hourly resolutions of the IMF, solar wind plasma data, energetic particle fluxes, and some solar and geomagnetic activity indices. It is a convenient and widely used source for the study of geomagnetic storms. The time interval under investigation is from January 1964 to July 2001, which is the most recent updated OMNI data set. During this time period, there are many times when solar wind data are not available. Thus we only use *Dst*, $VB_s$, and solar wind dynamic pressure $P$ data that have been continuously observed over at least 2 hours. We are left with ~80,000 data points for the northward $B_z$ and ~78,000 data points for the southward $B_z$. During the 37.5-year period of interest, hundreds of storms of different sizes and many periods of quiescent behavior were identified.

[10] In this section we will discuss the influence of the solar wind dynamic pressure on the ring current decay time when the IMF is orientated northward, namely $B_z \geq 0$. When the solar wind dynamic pressure increases, the magnetopause and the geomagnetic field lines in the Earth's radiation belt are pushed closer toward the Earth. Particles that make up the ring current drift are carried by the geomagnetic field lines, so that the position of the ring current will also move closer to the Earth as the solar wind dynamic pressure increases. If the ring current is closer to the Earth, the particles that make up the current will be exposed to a higher neutral density. This higher neutral density will increase the effective charge exchange rate or decrease the decay time $\tau$ of the ring current. With these considerations we will assume that the decay time of the ring current depends on the solar wind dynamic pressure $P$ when IMF is northward. However, other physical loss processes may also influence the ring current decay rate.

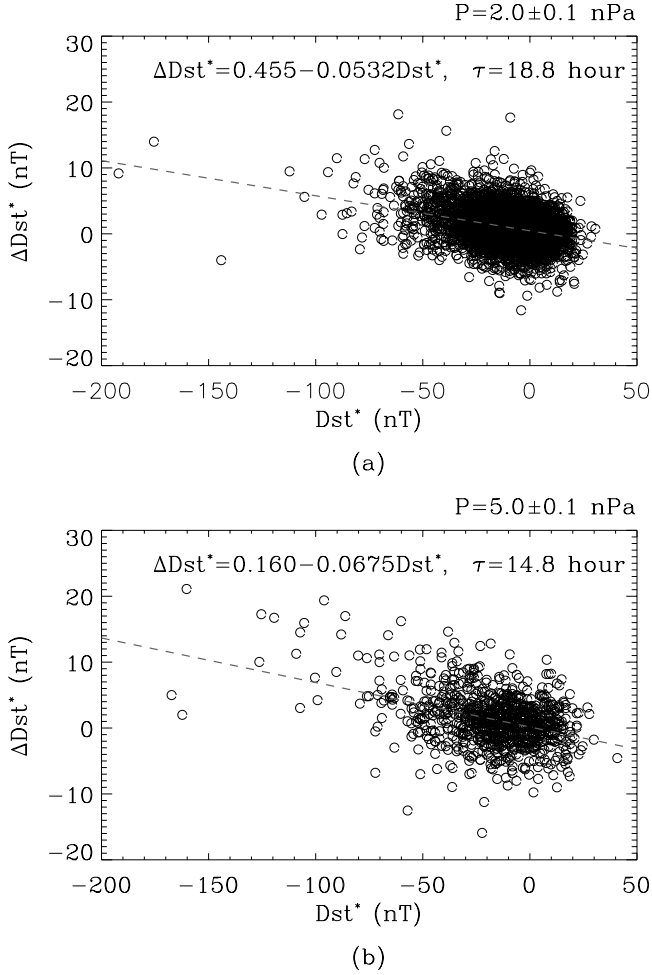


**Figure 1.** One-hour difference of *Dst** as a function of *Dst**, namely the pressure-corrected *Dst*, for two values of *P*: (a) $P = 2.0 \pm 0.1$ nPa and (b) $P = 5.0 \pm 0.1$ nPa. Here the range of *P* is indicated by ±0.1 nPa. The dashed line shows the linear least squares fit to the data points.

[11] From the Burton equation (equation (4)), one can express the hourly *Dst** difference as

$$\Delta Dst^* = Dst^*(t+1) - Dst^*(t) = Q(t) - Dst^*(t)\tau^{-1}. \quad (9)$$

Many *Dst** models with different pressure corrections have been derived. In this paper, the *O'Brien and McPherron* [2000a] result will be used

$$\Delta Dst^* = Dst - 7.26\sqrt{P} + 11\,\mathrm{nT}. \quad (10)$$

Here *P* and $\tau$ are in nanopascals (nPa) and hours, respectively. By assuming that $\tau$ is uniquely determined by *P* when $B_z \geq 0$, we linearly fit the $\Delta Dst^*$ variations against *Dst** for a given *P*. From the slopes of these lines, the values of $\tau$ are obtained.

[12] Figure 1 shows a scatterplot of the $\Delta Dst^*$ as a function of *Dst** for two values of *P*. The top and bottom panels of Figure 1 are for $P = 2.0 \pm 0.1$ nPa and $P = 5.0 \pm 0.1$ nPa, respectively. The dashed lines in Figure 1 indicate the linear least squares fit to the data points. The decay times $\tau$ are 18.8 and 14.8 hours for solar wind dynamic pressures equal to 2.0 and 5.0 nPa, respectively. In addition, the offset of both lines is nearly zero, which implies the ring current injection is very weak when the IMF is northward. This agrees with the observations that sufficiently large southward IMF values are a necessary condition for geomagnetic storms [*Gonzalez and Tsuratani*, 1987]. In this paper, we let $Q = 0$ during periods of the northward IMF.

[13] In Figure 2a we present the estimated decay time values, $\tau$ for the ring currents obtained with different solar wind dynamic pressure values, *P*. It is clearly shown that the ring current decay time decreases as the solar wind dynamic pressure increases, as would be expected from the above analysis. The decay time of the ring current decreases from ~25 hours for a small solar wind dynamic pressure to ~10 hours for a solar wind dynamic pressure >20 nPa. We have performed a least squares error fit to the estimated $\tau$, for *P* values between 0 and 20 nPa, using the same functional form as the one used by *O'Brien and McPherron* [2000a].

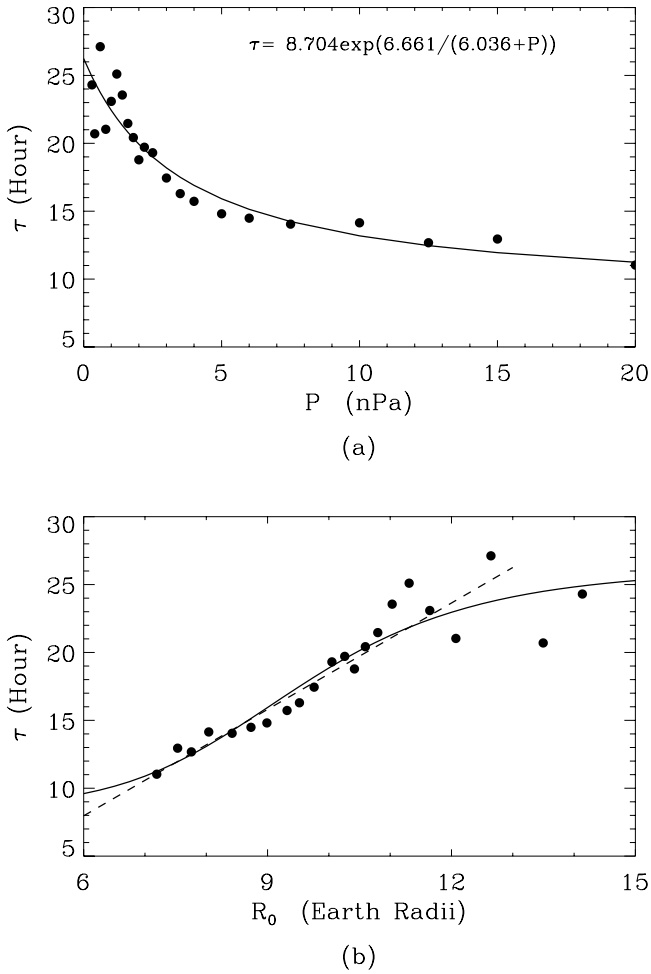


**Figure 2.** Decay time $\tau$ versus (a) the solar wind dynamic pressure *P* and (b) the geocentric distance $R_0$ of magnetopause subsolar point. The solid curve in Figure 2a represents the least squares fit to the data points. The data points and the solid curve in Figure 2b are replotted from Figure 2a by transforming *P* to $R_0$ with $R_0 = 11.646P^{-1/6.215}$ in $R_E$ [*Chao et al.*, 2002]. The dashed line in Figure 2b shows the least linear squares fit to the data points with $R_0 < 11\ R_E$.

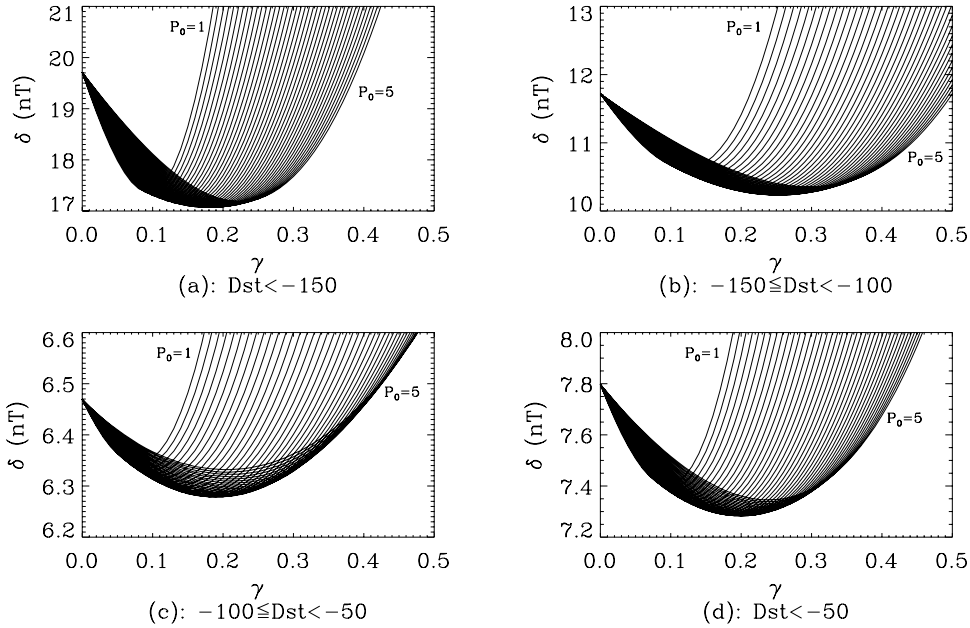


**Figure 3.** RMS errors between the measured $\Delta Dst$ and the calculated $\Delta Dst$ using equations (13a)–(13d) as a function of $\gamma$ for different $P_0$, separately for intervals of measured $Dst$: (a) $Dst < -150$ nT, (b) $-150$ nT $\leq Dst < -100$ nT, (c) $-100$ nT $\leq Dst < -50$ nT, and (d) $Dst < -50$ nT. The constant $P_0$ curve moves from the left to the right-hand side as $P_0$ increases from 1 to 5 nPa with an increment of 0.1 nPa in Figures 3a–3d.

This fit is shown in Figure 2a as the solid curve. The expression is

$$\tau = 8.70e^{6.66/(6.04+P)}. \tag{11}$$

The 18 hours result obtained by *O'Brien and McPherron* [2000a] for all northward IMF, equals the value of $\tau$ from equation (11) with $P \approx 3$ nPa, which is close to the average solar wind dynamic pressure value for our data set.

[14] To show the dependence of the ring current decay time on the size of the magnetosphere, the plot of $\tau$ as a function of the subsolar distance $R_0$ of the Earth's magnetopause is shown in Figure 2b, where $R_0 = 11646P^{-1/6.215}$ in Earth radii ($R_E$) [*Chao et al.*, 2002]. The result shows that the ring current decay time seems to decrease linearly as the size of the magnetopause $R_0$ decreases when $R_0$ is smaller than 11 $R_E$. If we compare Figure 2a with Figure 2b, it is easy to understand why $\tau$ decreases slowly with $P$, when $P$ is >5 nPa. The reason is that the size of the magnetopause $R_0$ changes only 1.25 times, from 9.0 $R_E$ to 7.2 $R_E$, while the solar wind dynamic pressure $P$ changes fourfold from 5 to 20 nPa. In addition, the result in Figure 2b suggests that the ring current decay time seems to approach a constant value of ~24 hours for a big magnetopause size, $R_0$ larger than 12 $R_E$. This is because the distance between the ring current and the Earth surface will not increase infinitely, although the magnetopause can become infinitely large in theory, when the solar wind dynamic pressure vanishes.

## 3. How Injection Depends on Solar Wind Dynamic Pressure

[15] Stimulated by the work of *Murayama* [1982] and *Fenrich and Luhmann* [1998], we propose that the injection of the ring current depends on the solar wind dynamic pressure in the form

$$Q = -4.4(VB_s - 0.49)\left(\frac{P}{P_0}\right)^{\gamma}. \tag{12}$$

Here $-4.4$ nT/(mV m$^{-1}$) and 0.49 mV m$^{-1}$ have been obtained by *O'Brien and McPherron* [2000a]. The power index, $\gamma$, and the $P_0$ will be optimized by minimizing the root-mean-square (RMS) errors of $\Delta Dst$ between the predicted one-step values and measured values of the hourly $Dst$ difference. For convenience, all the equations used in the optimization process can be rewritten as follows:

$$\begin{cases} dDst^*/dt = Q - Dst^*/\tau, & \text{(13a)} \\ Dst^* = Dst - 7.26\sqrt{P} + 11\text{nT}, & \text{(13b)} \\ Q = \begin{cases} 0 & VB_s \leq 0.49\,\text{mV/m} \\ -4.4(VB_s - 0.49)(P/P_0)^{\gamma}, & VB_s > 0.49\,\text{mV/m} \end{cases}, & \text{(13c)} \\ \tau = \begin{cases} 8.70e^{6.66/(6.04+P)}, & B_z \geq 0 \\ 2.40e^{9.74/(4.69+VB_s)}, & B_z < 0 \end{cases}. & \text{(13d)} \end{cases}$$

[16] In Figure 3 the RMS errors between the measured $\Delta Dst$ and the calculated $\Delta Dst$ using equations (13a)–(13d) are separately presented as a function of $\gamma$ for different $P_0$ for the measured $Dst$ intervals indicated at the bottom of each panel. In these calculations, all available points with continuous observations covering at least 2 hours of the $Dst$, $VB_s$, and solar wind dynamic pressure $P$ from the January 1964 to July 2001 OMNI database are included. The values

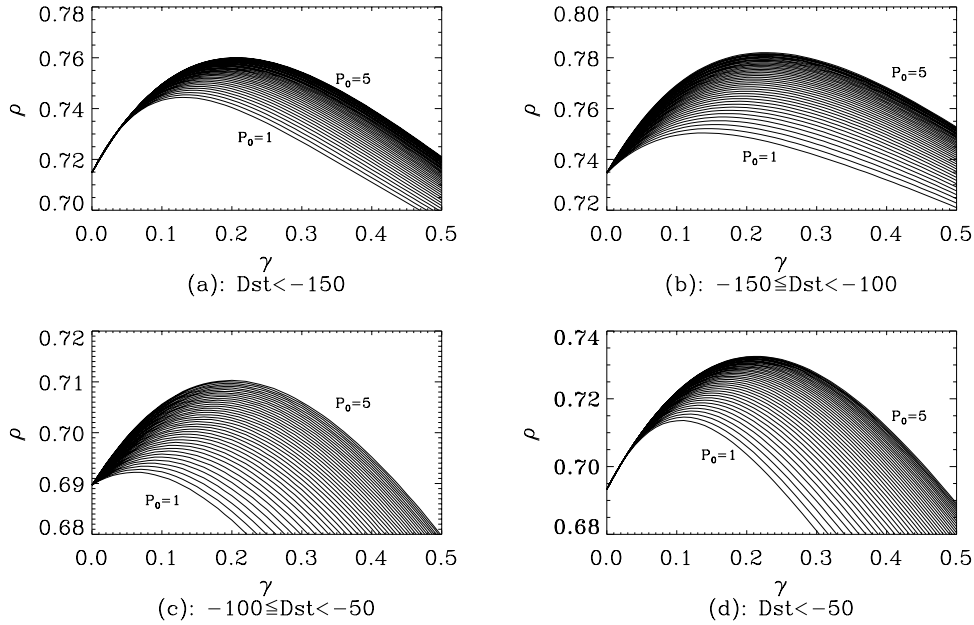


**Figure 4.** Linear correlation coefficients between the measured $\Delta Dst$ and the calculated $\Delta Dst$ for the same data points considered in Figure 3.

of $\gamma$ and $P_0$ change from 0 to 0.5 with an increment of 0.01 and from 0 to 5 nPa with an increment of 0.1 nPa, respectively. The different curves in each panel of Figure 3 show variations in the RMS errors versus $\gamma$ for different fixed values of $P_0$. The constant $P_0$ curve moves from the left-hand to the right-hand side, as can be seen in each plot, as $P_0$ increases from 1 to 5 nPa. We only display the results for measured *Dst* less than −50 nT, which is important for space weather prediction.

[17] For each curve, the RMS error $\delta$ first decreases with an increase of the power index $\gamma$, approaches a minimum value, then increases as $\gamma$ increases. There are some differences between these minimum $\delta$ values for different values of $P_0$, in each panel of Figure 3. It is found that the optimum values of $\gamma$ and $P_0$, when $\delta$ is at a minimum, are also slightly different for different measured *Dst* intervals, namely $(\gamma, P_0)_{\text{optm}}$ = (0.18, 3.5), (0.25, 3.5), (0.19, 3.1), and (0.2, 3.3) for Dst < −150 nT, and −150 nT ≤ *Dst* < −100 nT, −100 nT ≤ *Dst* < −50 nT, and *Dst* < −50 nT respectively.

[18] Figure 4 shows the linear correlation coefficients between the measured $\Delta Dst$ and the calculated $\Delta Dst$ for the data points considered in Figure 3. It is shown that the correlation coefficients reach a maximum at the range of $\gamma$ between 0.1 and 0.3. The maximum values are also different for different values of $P_0$, for different intervals of measured *Dst*. In general, in each panel of Figure 4 the maximum correlation coefficients increase with the increase of $P_0$. However, this growth is very slow when $P_0$ is >3.0 nPa, especially for strong magnetic storms.

[19] Fortunately, the optimum values of $\gamma$ and $P_0$ in Figures 3 and 4 are very close to each other, and it is possible to find a set of $(\gamma, P_0)_{optm}$, such that the minimum RMS errors and maximum correlation coefficients are satisfied. Finally, we choose

$$\gamma = 0.2, \quad P_0 = 3.0\,\text{nPa} \tag{14}$$

as the final and best values in equation (13c) for predicting the *Dst* variation from the observed solar wind parameters.

## 4. Applications to *Dst* Prediction

[20] In this section we will perform a comparison on the ability of multistep prediction of *Dst* between four models, namely our model using equations (13a)–(13d) and (14), the model of *O'Brien and McPherron* [2000a] (hereinafter referred to as the OM model), the model of *Fenrich and Luhmann* [1998] (hereinafter referred to as the FL model), and the model of *McPherron and O'Brien* [2001] (hereinafter referred to as the MO model). Both the FL model and our model include the influence of the solar wind dynamic pressure on the injection of the ring current, but the FL model is based on the old results of *Burton et al.* [1975]. The MO model considers that the pressure correction parameter $b$ is a function of $VB_s$. In the multistep prediction, after an initial *Dst* value is provided from ground measurements we use the model output from the previous hour as the initial starting *Dst* value for the following recursion until there is a solar wind data gap. It is found that the solar wind dynamic pressure plays a crucial role in the prediction of the *Dst*, especially for intense geomagnetic storms. To clearly show the influence of the solar wind dynamic pressure, we only show predictions for the OM model and our model for one moderate and two intense storms. Our model predictions are also better than those of the other two models for the three storms, which are not shown in the figures. Then, we give a more comprehensive comparison of all four models, based on the entire 37.5 years of OMNI data used in this study.

[21] First, we consider a moderate storm that occurred on 8–15 February 1997, illustrated by *Huttunen et al.* [2002], to investigate the variability of magnetospheric storms driven by different solar wind perturbations. Figure 5 presents the solar wind and the geophysical characteristics of this storm.

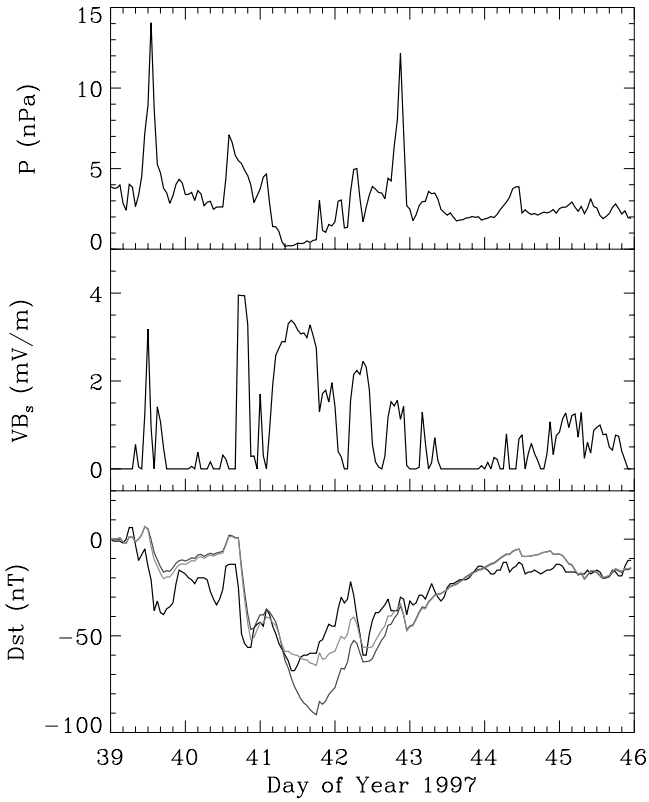


**Figure 5.** Solar wind and *Dst* parameters for a moderate storm on 8–15 February 1997. (top) Solar wind dynamic pressure *P* and (middle) dawn-dusk electric field $VB_s$. (bottom) Black, blue, and red curves representing the measured *Dst* and the multistep predicted *Dst* predicted by the *O'Brien and McPherron* [2000a] (OM) model and our model, respectively. Here all the data are hourly values. See color version of this figure at back of this issue.

All the data are from the OMNI database. Figure 5 shows (top, middle) the solar wind dynamic pressure *P* and the dawn-dusk electric field $VB_s$, respectively. Figure 5 (bottom) shows the measured *Dst* (black curve), the *Dst* calculated using the OM model (blue curve), and our model (red curve). During the period 0700–1800 UT on 10 February the solar wind dynamic pressure was extremely low, between 0.1 and 0.6 nPa. At the same time, $VB_s$ is $\sim$3 mV m$^{-1}$. It is clear from this plot that our model reproduces almost the same minimum measured *Dst* values for this period, while the OM model predicts a *Dst* of $-91$ nT, nearly 1.34 times the amplitude of the observed minimum value. This discrepancy is consistent with the result of equation (13c) that the ring current injection should decrease for a lower solar wind dynamic pressure.

[22] Second, we consider two strong storms that occur during the period from 30 March to 15 April 2001. The solar wind parameters and the geomagnetic index are presented in Figure 6 in a format similar to that of Figure 5. During this period, there are many solar wind data gaps in the OMNI database. Thus we use hourly averages of the solar wind plasma and IMF data from the Solar Wind Electron Proton Alpha Monitor and magnetometer instruments, on board the ACE satellite in Figure 6. A time lag of $\Delta t = \Delta x/V_{sw}$ has been adjusted for propagation from ACE to the Earth, where $\Delta x$ is the distance between the position of ACE and the Earth and $V_{sw}$ is the solar wind speed. A common characteristic of these two storms is that the solar wind dynamic pressures were very high during the main phase of the storms; these intense solar wind dynamic pressures greatly enhanced the injection of the ring current during the storms, as expected from equation (13c). Our model (red curve in Figure 5) reproduces the *Dst* variations very well, both in the main phase and in the recovery phase, as well as the minimum values of the measured *Dst*. On the other hand, the OM model (blue curve in Figure 5) seriously underestimates the minimum values for both storms. The minimum values obtained by the OM model are $-246$ nT and $-168$ nT, which are $\sim$69% and 66% of the observed minimum values, and -358 nT and $-256$ nT, for the first and the second storms, respectively. The resulting prediction efficiencies of our model are 98% (RMS error 13.9 nT) and 89% (RMS error 13.8 nT), which are higher than the OM model results, 94% (RMS error 33.5 nT) and 83% (RMS error 18.3 nT), for the first and second storms, respectively.

[23] Finally, we scanned the entire 37.5-year OMNI database, identifying all intervals with continuous solar wind observations covering at least of 12 hours. There are in total 3041 intervals with $\sim$130,200 data points. For each of these intervals we start the integration from a known initial *Dst* value and integrate to the end of the interval using multistep prediction feedback. Then, we analyze the RMS

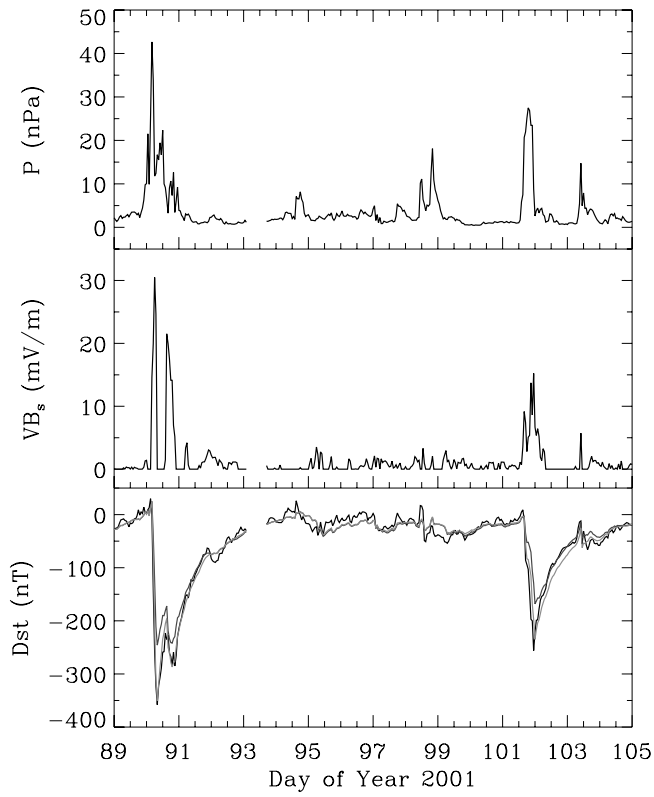


**Figure 6.** Solar wind and *Dst* parameters for two intense storms during the period from 30 March to 15 April 2001 with the same format as in Figure 5. See color version of this figure at back of this issue.

**Table 1.** RMS Errors Between Measured *Dst* and Multistep Predicted *Dst* for Different Measured *Dst* Intervals[a]

| | RMS Errors, nT | | | | | | | |
|---|---|---|---|---|---|---|---|---|
| | *Dst*, nT, $\geq 0$ | *Dst*, nT, $-50 \sim 0$ | *Dst*, nT, $-100 \sim 50$ | *Dst*, nT, $-150 \sim 100$ | *Dst*, nT, $<-150$ | *Dst*, nT, $<0$ | *Dst*, nT, $<-50$ | *Dst*, nT, All |
| FL model | 8.16 (1.146) | 13.43 (0.773) | 25.80 (0.396) | 33.57 (0.286) | 71.47 (0.362) | 15.01 (0.706) | 28.75 (0.393) | 13.78 (0.761) |
| MO model | 8.57 (1.204) | 12.53 (0.721) | 20.58 (0.316) | 28.81 (0.246) | 46.01 (0.233) | 13.46 (0.633) | 22.45 (0.307) | 12.54 (0.692) |
| OM model | 11.49 (1.615) | 8.80 (0.506) | 16.57 (0.254) | 28.25 (0.241) | 58.84 (0.298) | 10.01 (0.471) | 20.15 (0.276) | 10.36 (0.572) |
| Our model | 11.28 (1.585) | 8.63 (0.496) | 15.64 (0.240) | 21.05 (0.179) | 31.92 (0.162) | 9.43 (0.443) | 16.80 (0.230) | 9.87 (0.545) |

[a]Values in parenthses are relative errors equal to the ratios of RMS error divided by the mean value of absolute measured *Dst* in the corresponding interval. FL, *Fenrich and Luhmann* [1998]; MO, *McPherron and O'Brien* [2001]; OM, *O'Brien and McPherron* [2000a].

errors and correlation coefficients between the measured *Dst* and the calculated *Dst* by combining all the available data points together. This technique allows us to attain a much more comprehensive comparison of the prediction ability of the different models, based on a large number of storms of different sizes. This is in contrast to previous comparisons based on one or a few storms [e. g., *O'Brien and McPherron*, 2000b; *Feldstein*, 1992, and references therein].

[24] Table 1 shows the RMS errors between the calculated *Dst* and the measured *Dst* for the above four models, for different measured *Dst* intervals. The relative error, defined as the ratio of the RMS error divided by the corresponding average, is given in parentheses in Table 1. One can see that the RMS errors for the measured negative *Dst* obtained using our model are always smaller than the corresponding values obtained from the other three models. In particular, compared to the values of the OM model, the RMS errors of our model decrease significantly for intense storms, e.g., from 28.25 to 21.05 nT (a decreasing of 25%) for the *Dst* range from $-150$ nT $\leq Dst < -100$ nT and from 58.84 to 31.92 nT (a 46% decrease), when the $Dst < -150$ nT. The RMS errors are 20.15 nT and 16.80 nT for the OM model and our model, respectively, when the measured Dst is smaller than $-50$ nT. However, the RMS errors for all measured *Dst* decrease only slightly, from 10.36 to 9.87 nT, because 93% of the measured *Dst* is greater than $-50$ nT when our model does not show much improvement over the OM model. In general, the OM model is better than the FL and MO models, even though the RMS error of the MO model is smaller then the error of the OM model for strong storms ($Dst < -150$ nT). However, the FL and the MO models are better than either the OM or our model in terms of positive measured *Dst*.

[25] Table 2 shows the correlation coefficients between the measured and calculated *Dst* for the four models, using exactly the same data points as in Table 1. The results indicate that the correlation coefficients of our model are the highest among the four when the measured *Dst* is negative. Comparing the OM model with our model, the correlations of our model increase from 0.591 to 0.635, from 0.374 to 0.551, from 0.573 to 0.746, and from 0.789 to 0.868 for *Dst* in the range of $-100$ nT $\leq Dst < -50$ nT, $-150$ nT $\leq Dst < -100$ nT, $Dst < -150$ nT, and $Dst < -50$ nT, respectively. The global correlation coefficients of all the *Dst* are 0.891 for our model, which is the largest among the four models. For moderate storms ($-100$ nT $\leq Dst < -0$ nT) the correlation coefficients of the OM model are higher than the values of the FL and MO models. However, for intense storms ($Dst < -100$ nT), the correlation coefficients of the FL model are higher than the values of the MO model, which are in turn higher than the values of the OM model. Therefore we suggest that the importance of the solar wind dynamic pressure influence on intense geomagnetic storms does exist.

[26] In summary, it is clearly shown from the above analysis that the solar wind dynamic pressure plays an important role in the coupling between the solar wind and the magnetosphere. By including the influences of the solar wind dynamic pressure, the *Dst* prediction of OM model can be substantially improved, especially for intense geomagnetic storms.

## 5. Discussion

[27] One can see from Tables 1 and 2 that neither our model nor the OM model can predict positive *Dst* variations very well when the RMS errors between the measured and calculated *Dsts* are $\sim$1.6 times the average measured *Dst* value. One interesting result is that for both models the RMS errors decrease sharply to a value $\sim$0.9 times the average measured *Dst* value for measured positive *Dst* if we artificially let $c$ be equal to zero in the pressure corrected *Dst* expression but keep all the other parameters in the calculation unchanged. Of course, this will increase the RMS errors for negative measured *Dst*. However, the global correlation coefficient (RMS errors) between the measured *Dst* and the calculated *Dst*, using a multistep prediction, will increase (decrease) to 0.912 (8.87 nT) when our model is modified as follows: We first calculate the *Dst* variations for

**Table 2.** Correlation Coefficients Between Measured *Dst* and Multistep Predicted *Dst* for Different Measured *Dst* Intervals

| | Correlation Coefficients | | | | | | | |
|---|---|---|---|---|---|---|---|---|
| | *Dst*, nT, $\geq 0$ | *Dst*, nT, $-50 \sim 0$ | *Dst*, nT, $-100 \sim -50$ | *Dst*, nT, $-150 \sim -100$ | *Dst*, nT, $<-150$ | *Dst*, nT, $<0$ | *Dst*, nT, $<-50$ | *Dst*, nT, All |
| FL model | 0.511 | 0.633 | 0.483 | 0.476 | 0.695 | 0.814 | 0.786 | 0.821 |
| MO model | 0.472 | 0.679 | 0.550 | 0.438 | 0.576 | 0.827 | 0.792 | 0.847 |
| OM model | 0.473 | 0.749 | 0.591 | 0.374 | 0.573 | 0.866 | 0.789 | 0.879 |
| Our model | 0.480 | 0.757 | 0.635 | 0.551 | 0.746 | 0.886 | 0.868 | 0.891 |

both cases of $c = 0$ nT and $c = 11$ nT, respectively, and then assign the calculated *Dst* from the $c = 0$ nT case if the measured *Dst* is positive, otherwise using the calculated *Dst* from $c = 11$ nT. Such a mixed model seems to improve the *Dst* prediction. The constant $c$ represents the contribution of the quiet time currents in the magnetosphere to the *Dst* index. This result seems to suggest that the contribution of the quiet time currents to the *Dst* index is at least not negative, implying that the contribution from the quiet time current may be negligible.

[28] In section 2 we found that the solar wind dynamic pressure influences the decay time $\tau$ of the ring current for a northward orientated IMF. Does this influence still exist for a southward IMF? Basically, the answer should be positive. To derive such a decay time dependence as a function of both the solar wind dynamic pressure and dawn-dusk electric field, a large database is needed. However, in this study we postulate that $\tau$ is not influenced significantly by the solar wind dynamic pressure during the southward IMF, especially with strong negative $B_z$ when the position of the ring current is mainly controlled by the convection pattern of the hot ions that make up the ring current as suggested by *O'Brien and McPherron* [2000a].

[29] Why is the injection of ring current influenced by the solar wind dynamic pressure? We are giving some physical interpretations as follows. First, the energy-coupling function between the solar wind and the magnetosphere can be expressed as [*Vasyliunas et al.*, 1982]

$$P_{in} = \frac{VB^2}{2\mu_0} L_{CF}^2 M_A^{2\alpha} F(\theta) \propto V^{2\alpha+1/3} B^{2-2\alpha} \rho^{\alpha-1/3}, \qquad (15)$$

where $B$, $\theta$, $V$ and $\rho$ are the magnitude and an equivalent clock angle of interplanetary magnetic field, the solar wind velocity and mass density, respectively, and $M_A$ is the solar wind Alfvén Mach number. The equation $L_{CF} = (M_e^2/\rho V^2)^{1/6}$ scales as the Chapman-Ferraro magnetopause distance, where $M_e$ is the Earth's dipole moment. By adjusting the dimensionless parameter $\alpha$ our energy injection function of ring current $Q \sim VB_sP^{1/5}$ is in very good agreement with $P_{in} \sim VB^{14/15}P^{1/5}$ with $\alpha = 8/15$. This seems to imply that the solar wind energy transfers to the magnetosphere mainly due to mass flow along the open field lines across the rotational magnetopause structures [*Kan and Akasofu*, 1982]. Second, *Alexeev et al.* [1996] and *Turner et al.* [2000] found that the cross-tail current could have a significant contribution to the *Dst* index. An increase in the solar wind dynamic pressure will increase the tail field thus also increase the tail current. This effect is modeled by adding a dependence on solar wind dynamic pressure in the injection term of the Burton equation (equation (4)). Third, injection strength of the ring current theoretically depends on the strength of the $\mathbf{E} \times \mathbf{B}$ convection in the nightside magnetosphere and the inner plasma sheet density (the source population of ring current). On one hand, the magnetic field in the magnetosphere will increase when the solar wind dynamic pressure increases, so the $\mathbf{E} \times \mathbf{B}$ convection can become stronger, and the injection of ring current is enhanced. Furthermore, simulation studies have shown that by using a drift-loss kinetic transport ring current model an increase in the density of the inner plasma sheet produces an enhancement in the strength of the simulated ring current [e.g., *Chen et al.*, 1994; *Kozyra et al.*, 1998; *Liemohn et al.*, 2001]. *Thomsen et al.* [1998] examined a set of 23 geomagnetic storms that occurred during 1997 and 1998 with minimum *Dst* ranging from $-47$ to $-166$ nT. They found that there exists a relationship between the strength of the storm time ring current and, independently, both $VB_s$ and the plasma sheet density observed at geosynchronous orbit. In addition, *Borovsky et al.* [1998] demonstrated a strong correlation between the solar wind density and the plasma sheet density, measured both at geosynchronous orbit and in the midtail neutral sheet region. These observation and simulation results seem to support a picture in which the solar wind density may be an additional driver of ring current by determining the plasma sheet density [*Smith et al.*, 1999]. However, *O'Brien and McPherron* [2000c] show that there is no statistical signal for an independent solar wind density driver of the terrestrial ring current by studying the bilinear correlation of the minimum *Dst* respect to $VB_s$ and solar wind density for 439 storms identified from a set of over 30 years of OMNI database. The result of *O'Brien and McPherron* [2000c] is likely to indicate that enhancement of ring current injection with high solar wind dynamic pressure is not directly due to the transport of high-density solar wind material to nightside near-Earth plasma sheet and then to the ring current. Our *Dst* prediction results show that the enhancement of ring current injection with high solar wind dynamic pressure is most important for intense-to-great geomagnetic storms. Composition studies have shown that the ionosphere contributes significantly to the storm time ring current for strong storms [e.g., *Daglis*, 1997]. Does a higher solar wind dynamic pressure produce a stronger injection of ionosphere plasma to the inner plasma sheet and also to the ring current? Verification of this is beyond the scope of this investigation. Finally, it is shown in section 2 that the ring current decays faster with higher solar wind dynamic pressure for northward IMF since the position of ring current is compressed closer to the Earth surface. We suggest that, according to the conservation of the third adiabatic invariant, both the open and closed drift trajectories of the ring current particles can move nearer to the Earth with an increase of the solar wind dynamic pressure for southward IMF. At the same time, the ring current particles are energized so that the injection of ring current can be enhanced. However, this increase of ring current energy may be weakened by the high loss rate of energy for a low-altitude ring current. A simulation using the drift-loss ring current model, such as *Chen et al.* [1994], *Kozyra et al.* [1998], and *Liemohn et al.* [2001], will be helpful to understand this issue.

[30] The nonlinear response of the ionosphere-magnetosphere coupling to the solar wind conditions has been studied in numerous works in which the algorithm of *Burton et al.* [1975] (hereinafter referred to as B75) has often been used to demonstrate that there is a ring current saturation on convection electric field [e.g., *Russell et al.*, 2001; *Liemohn et al.*, 2002; *Liemohn and Ridley*, 2002]. The 24–25 September 1998 storm was chosen by *Liemohn and Ridley* [2002] as an example of ring current saturation due to ionosphere-magnetosphere coupling. In Figure 7 we present the observed *Dst* and the B75 model, OM model, and our model predictions for this storm. It is found that the

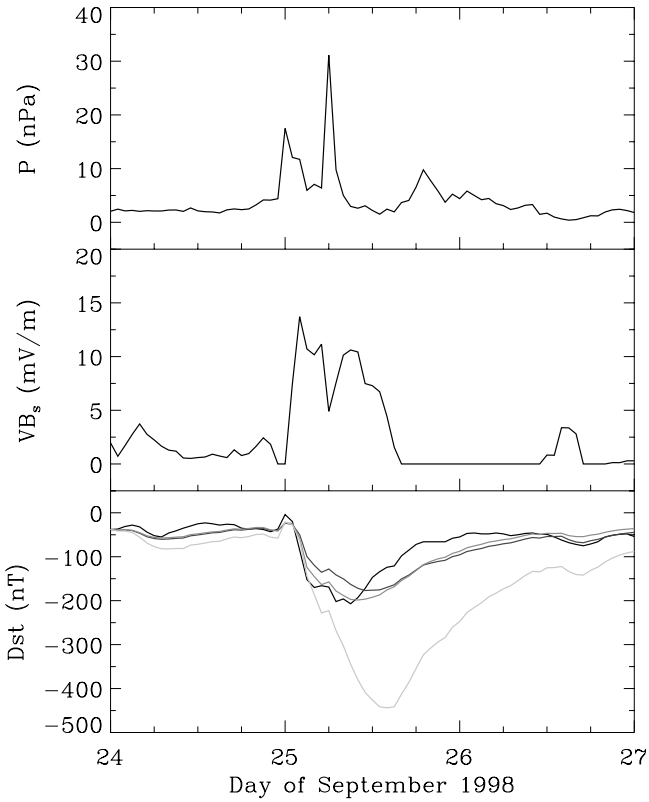


**Figure 7.** Solar wind and *Dst* parameters for the 24–27 September 1998 storm with the same format as in Figure 5. (bottom) Black, blue, red, and green curves representing the measured *Dst* and the multistep predicted *Dst* predicted by the OM model, our model, and the *Burton et al.* [1975] (B75) algorithm, respectively. When using higher resolution data, the B75 model also overestimates the minimum measured *Dst* value as shown in Figure 4 of *Liemohn and Ridley* [2002]. See color version of this figure at back of this issue.

minimum value of the measured *Dst* is seriously overestimated by the B75 model, but is underestimated by the OM model, when the injection of the ring current is both linearly proportional to the interplanetary electric field $VB_s$. The main reason for this difference is that the decay time is much smaller in the OM model (~4 hours) than in the B75 model (~17 hours) when $VB_s \approx 10$ mV m$^{-1}$. On the other hand, due to the injection increase from the large solar wind dynamic pressure, our model predicts the variation in the measured *Dst* much better than the other two models.

## 6. Conclusions

[31] In this paper, the influences of solar wind dynamic pressure on the decay time and the injection of the ring current are investigated using the OMNI data for the period from January 1964 to July 2001. The main results are summarized as follows.

[32] 1. The decay time, $\tau$, of the ring current is controlled by the size of the magnetosphere for northward IMF. It is found that $\tau$ decreases as the solar wind dynamic pressure increases, interpreted as the same as a decrease of the magnetospheric size during the periods of northward IMF.

[33] 2. The strength of the ring current injection is proportional to the solar wind dynamic pressure with a power index of 0.2 during southward IMF. This implies that the ring current injection increases when the magnetosphere is more compressed by high solar wind dynamic pressure.

[34] 3. The *Dst* prediction model of *O'Brien and McPherron* [2000a] can be significantly improved by considering the influence of solar wind dynamic pressure, especially for strong geomagnetic storms.

[35] **Acknowledgments.** This work was supported by the National Science Council of the Republic of China under grant NSC 91-2111-M-008-026 at the National Central University. C.B.W is grateful for the support of the National Research Council as a visiting scientist at the Institute of Space Sciences, National Central University, under grant NSC 91-2816-M-008-0008-6 and also acknowledges the support of the National Science Foundation of China under grant 40004006. J.K.C would like to thank R. L. McPherron for his helpful discussions. C.B.W is thankful for the support and encouragement of S. Wang and C. S. Wu for a visitor exchange program between the National Central University and University of Science and Technology of China. The interplanetary data and the geomagnetic indices, *Kp* and *Dst*, are from the OMNI database of the U.S. National Space Science Data Center. We also thank Ruth Skoug and the ACE spacecraft team for the ACE solar wind and magnetic field data.

[36] Lou-Chuang Lee thanks Margaret W. Chen and the other reviewer for their assistance in evaluating this paper.

## References

Akasofu, S.-I., The energy coupling between the solar wind and the magnetosphere, *Space Sci. Rev.*, *28*, 121–190, 1981.

Akasofu, S.-I., and S. Chapman, *Solar-Terrestrial Physics*, Oxford Univ. Press, New York, 1972.

Alexeev, I. I., E. S. Belenkaya, V. V. Kalegaev, Y. I. Feldstein, and A. Grafe, Magnetic storms and magnetotail currents, *J. Geophys. Res.*, *101*, 7737–7747, 1996.

Borovsky, J. E., M. F. Thomsen, and R. C. Elphic, The driving of the plasma sheet by the solar wind, *J. Geophys. Res.*, *103*, 17,617–17,639, 1998.

Burton, R. K., R. L. McPherron, and C. T. Russell, An empirical relationship between interplanetary conditions and *Dst*, *J. Geophys. Res.*, *80*, 4204–4214, 1975.

Campbell, W. H., Geomagnetic storms, the *Dst* ring-current myth and lognormal distributions, *J. Atmos. Terr. Phys.*, *58*, 1171–1187, 1996.

Chao, J. K., D. J. Wu, C.-H. Lin, Y. H. Yang, X. Y. Wang, M. Kessel, S. H. Chen, and R. P. Lepping, Models for the size and shape of the Earth's magnetopause and bow shock, in *Space Weather Study Using Multipoint Techniques*, *COSPAR Colloquia Ser.*, vol. 12, edited by L. H. Lyu, pp. 127–135, Elsevier Sci., New York, 2002.

Chen, M. W., L. R. Lyons, and M. Schulz, Simulation of phase space distributions of storm time proton ring current, *J. Geophys. Res.*, *99*, 5745–5759, 1994.

Cowley, S. W. H., Pitch angle dependence of the charge-exchange lifetime of ring current ions, *Planet. Space Sci.*, *25*, 385–393, 1977.

Daglis, I. A., The role of magnetosphere-ionosphere coupling in magnetic storm dynamics, in *Magnetic Storms*, *Geophys. Monogr. Ser.*, vol. 98, edited by B. T. Tsurutani et al., pp. 107–116, AGU, Washington, D. C., 1997.

Daglis, I. A., and W. I. Axford, Fast ionosphere response to enhanced activity in geospace: Ion feeding of the inner magnetotail, *J. Geophys. Res.*, *101*, 5047–5065, 1996.

Daglis, I. A., E. T. Sarris, and B. Wilken, AMPTE/CCE CHEM observations of the magnetic ion population at geosynchronous altitudes, *Ann. Geophys.*, *11*, 685–696, 1993.

Daglis, I. A., R. M. Thorne, W. Baumjohann, and S. Orsini, The terrestrial ring current: Origin, formation, and decay, *Rev. Geophys.*, *37*, 407–438, 1999.

Dasso, S., D. Gómez, and C. H. Mandrini, Ring current decay rates of magnetic storms: A statistical study from 1957 to 1998, *J. Geophys. Res.*, *107*(A5), 1059, doi:10.1029/2000JA000430, 2002.

Dessler, A. J., and E. N. Parker, Hydromagnetic theory of magnetic storms, *J. Geophys. Res.*, *64*, 2239–2259, 1959.

Feldstein, Y. I., Modeling of the magnetic field of magnetospheric ring current as a function of interplanetary medium parameters, *Space Sci. Rev.*, *59*, 83–165, 1992.

Fenrich, F. R., and J. G. Luhmann, Geomagnetic response to magnetic clouds of different polarity, *Geophys. Res. Lett.*, *25*, 2999–3002, 1998.

Fok, M.-C., J. U. Kozyra, A. F. Nagy, and T. E. Cravens, Lifetime of ring current particles due to Coulomb collisions in the plasmasphere, *J. Geophys. Res.*, *96*, 7861–7867, 1991.

Fok, M.-C., T. E. Moore, J. U. Kozyra, G. C. Ho, and D. C. Hamilton, Three-dimensional ring current decay model, *J. Geophys. Res.*, *100*, 9619–9632, 1995.

Friedrich, E., G. Rostoker, M. G. Connors, and R. L. McPherron, Influence of the substorm current wedge on the *Dst* index, *J. Geophys. Res.*, *104*, 4567–4575, 1999.

Gonzalez, W. D., and B. T. Tsuratani, Criteria of interplanetary parameters causing intense magnetic storms, *Planet. Space Sci.*, *35*, 1101–1109, 1987.

Gonzalez, W. D., B. T. Tsurutani, A. L. C. Gonzalez, E. J. Smith, F. Tang, and S.-I. Akasofu, Solar wind-magnetosphere coupling during intense magnetic storms (1978–1979), *J. Geophys. Res.*, *94*, 8835–8851, 1989.

Gonzalez, W. D., J. A. Joselyn, Y. Kamide, H. W. Kroehl, G. Rostoker, B. T. Tsurutani, and V. M. Vasyliunas, What is a geomagnetic storm?, *J. Geophys. Res.*, *99*, 5771–5792, 1994.

Greenspan, M. E., and D. C. Hamilton, A test of the Dessler-Parker-Sckopke relation during magnetic storms, *J. Geophys. Res.*, *105*, 5419–5430, 2000.

Hakkinen, L. V. T., T. I. Pulkkinen, H. Nevanlinna, R. J. Pirjola, and E. I. Tanskanen, Effects of induced currents on *Dst* and magnetic variations at midlatitude stations, *J. Geophys. Res.*, *107*(A1), 1014, doi:10.1029/2001JA900130, 2002.

Hamilton, D. C., G. Gloeckler, R. M. Ipavivh, W. Studemann, B. Wilken, and G. Kremser, Ring current development during the great geomagnetic storms of February 1986, *J. Geophys. Res.*, *93*, 14,343–14,355, 1988.

Huttunen, K. E. J., H. E. J. Koskinen, and R. Schwenn, Variability of magnetospheric storms driven by different solar wind perturbations, *J. Geophys. Res.*, *107*(A7), 1121, doi:10.1029/2001JA900171, 2002.

Jordanova, V. K., J. U. Kozyra, and A. F. Nagy, Effects of heavy ions on the quasi-linear diffusion coefficients from resonant interactions with electromagnetic ion cyclotron waves, *J. Geophys. Res.*, *101*, 19,771–19,778, 1996.

Jordanova, V. K., C. J. Farrugia, J. M. Quinn, R. M. Thone, K. W. Ogilvie, R. P. Lepping, G. Lu, A. J. Lazarus, M. F. Thomsen, and R. D. Belian, Effect of wave-particle interactions on ring current evolution for January 10–11, 1997: Initial results, *Geophys. Res. Lett.*, *25*, 2971–2974, 1998.

Kamide, Y., et al., Current understanding of magnetic storms: Storm-substorm relationships, *J. Geophys. Res.*, *103*, 17,705–17,728, 1998.

Kan, J. R., and S.-I. Akasofu, Dynamo process governing solar wind-magnetosphere energy coupling, *Planet. Space Sci.*, *30*, 367–370, 1982.

Kozyra, J. U., V. K. Jordanova, J. E. Borovsky, M. F. Thomsen, D. J. Knipp, D. S. Evans, D. J. McComas, and T. E. Cayton, Effects of a high-density plasma sheet on ring current development during the November 2–6, 1993, magnetic storm, *J. Geophys. Res.*, *103*, 26,285–26,305, 1998.

Langel, R. A., and R. H. Estes, Large-scale, near-Earth magnetic fields from external sources and the corresponding induced internal field, *J. Geophys. Res.*, *90*, 2487–2494, 1985.

Liemohn, M. W., and A. J. Ridley, Comment on "Nonlinear response of the polar ionosphere to large values of the interplanetary electric field" by C.T. Russell et al., *J. Geophys. Res.*, *107*(A12), 1460, doi:10.1029/2002JA009440, 2002.

Liemohn, M. W., J. U. Kozyra, V. K. Jordanova, G. V. Khazanov, M. F. Thomsen, and T. E. Cayton, Analysis of early phase ring current recovery mechanisms during geomagnetic storms, *Geophys. Res. Lett.*, *26*, 2845–2848, 1999.

Liemohn, M. W., J. U. Kozyra, M. F. Thomsen, J. L. Roeder, G. Lu, J. E. Borovsky, and T. E. Cayton, Dominant role of the asymmetric ring current in producing the stormtime *Dst**, *J. Geophys. Res.*, *106*, 10,883–10,904, 2001.

Liemohn, M. W., J. U. Kozyra, M. R. Hairston, D. R. Weimer, G. Lu, A. J. Ridley, T. H. Zurbuchen, and R. M. Skoug, Consequences of a saturated convection electric field on the ring current, *Geophys. Res. Lett.*, *29*(9), 1348, doi:10.1029/2001GL014270, 2002.

Maezawa, K., and T. Murayama, Solar wind velocity effects on the auroral zone magnetic disturbances, in *Solar Wind-Magnetosphere Coupling*, edited by Y. Kamide and J. A. Slavin, pp. 59–83, Terra Sci., Tokyo, 1986.

McPherron, R. L., and T. P. O'Brien, Predicting geomagnetic activity: The *Dst* index, in *Space Weather*, *Geophys. Monogr. Ser.*, vol. 125, edited by P. Song, H. J. Singer, and G. L. Siscoe, pp. 339–345, AGU, Washington, D. C., 2001.

Murayama, T., Coupling function between solar wind parameters and geomagnetic indices, *Rev. Geophys.*, *20*, 623–629, 1982.

Murayama, T., Coupling functions between the solar wind and *Dst* index, in *Solar Wind-Magnetosphere Coupling*, edited by Y. Kamide and J. A. Slavin, pp. 111–117, Terra Sci., Tokyo, 1986.

O'Brien, T. P., and R. L. McPherron, An empirical phase space analysis of ring current dynamics: Solar wind control of injection and decay, *J. Geophys. Res.*, *105*, 7707–7719, 2000a.

O'Brien, T. P., and R. L. McPherron, Forecasting the ring current index *Dst* in real time, *J. Atmos. Sol. Terr. Phys.*, *62*, 1295–1299, 2000b.

O'Brien, T. P., and R. L. McPherron, Evidence against an independent solar wind density driver of the terrestrial ring current, *Geophys. Res. Lett.*, *27*, 3797–3799, 2000c.

Perreault, P. D., and S.-I. Akasofu, A study of geomagnetic storms, *Geophys. J. R. Astron. Soc.*, *54*, 547–573, 1978.

Prigancová, A., and Y. I. Feldstein, Magnetospheric storm dynamics in terms of energy input rate, *Planet. Space Sci.*, *40*, 581–588, 1992.

Roeder, J. L., J. F. Fennell, M. W. Chen, M. Schultz, M. Grande, and S. Livi, CRRES observations of the composition of ring current populations, *Adv. Space Res.*, *17*(10), 17–24, 1996.

Rostoker, G., E. Friedrich, and M. Dobbs, Physics of magnetic storms, in *Magnetic Storms*, *Geophys. Monogr. Ser.*, vol. 98, edited by B. T. Tsurutani et al., pp. 149–160, AGU, Washington, D. C., 1997.

Russell, C. T., J. G. Luhmann, and G. Lu, Nonlinear response of the polar ionosphere to large values of the interplanetary electric field, *J. Geophys. Res.*, *106*, 18,495–18,504, 2001.

Sckopke, N., A general relation between the energy of trapped particles and the disturbance field near the Earth, *J. Geophys. Res.*, *71*, 3125–3130, 1966.

Smith, J. P., M. F. Thomsen, J. E. Borovsky, and M. Collier, Solar wind density as a driver for the ring current in mild storms, *Geophys. Res. Lett.*, *26*, 1797–1800, 1999.

Smith, P. H., and N. K. Bewtra, Charge exchange lifetimes for ring current ions, *Space Sci. Rev.*, *22*, 310–318, 1978.

Smith, P. H., N. K. Bewtra, and R. A. Hoffman, Inference of the ring current ion composition by means of charge exchange decay, *J. Geophys. Res.*, *86*, 3470–3480, 1981.

Thomsen, M. F., J. E. Borovsky, D. J. McComas, and M. R. Collier, Variability of the ring current source population, *Geophys. Res. Lett.*, *25*, 3481–3484, 1998.

Tsurutani, B. T., J. A. Slavin, Y. Kamide, R. D. Zwickl, J. H. King, and C. T. Russell, Coupling between the solar wind and the magnetosphere: CDAW 6, *J. Geophys. Res.*, *90*, 1191–1199, 1985.

Turner, N. E., D. N. Baker, T. I. Pulkkinen, and R. L. McPherron, Evaluation of the tail current contribution to *Dst*, *J. Geophys. Res.*, *105*, 5431–5439, 2000.

Vasyliunas, V. M., J. R. Kan, G. L. Siscoe, and S.-I. Akasofu, Scaling relations governing magnetospheric energy transfer, *Planet. Space Sci.*, *30*, 359–365, 1982.

J. K. Chao and C. B. Wang, Institute of Space Science, National Central University, Jung-li 32001, Taiwan. (jkchao@sedc.ss.ncu.edu.tw; cbwang@ustc.edu.cn)

C.-H. Lin, Department of Electrical Engineering, Ching-Yun Institute of Technology, Jung-li 32001, Taiwan. (chlin@mail.njtc.edu.tw)

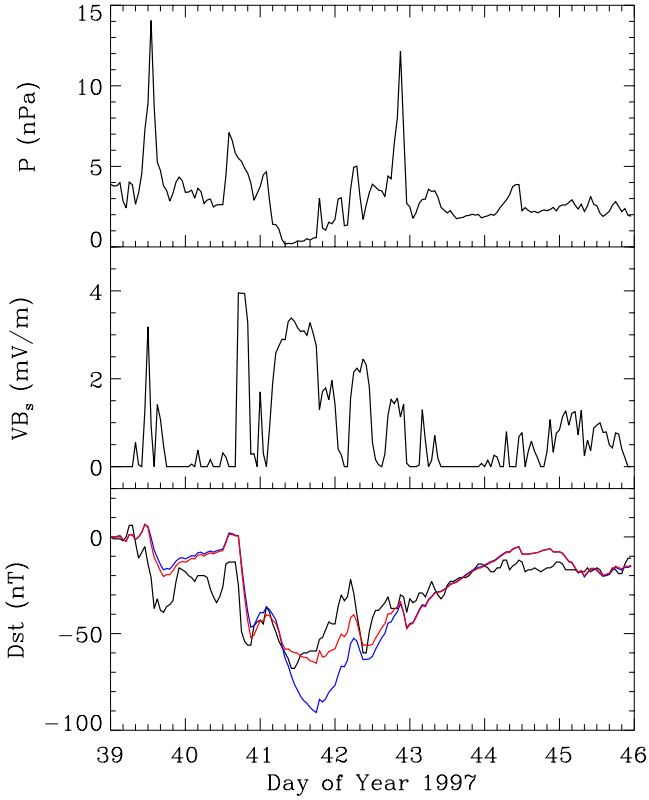


**Figure 5.** Solar wind and *Dst* parameters for a moderate storm on 8–15 February 1997. (top) Solar wind dynamic pressure $P$ and (middle) dawn-dusk electric field $VB_s$. (bottom) Black, blue, and red curves representing the measured *Dst* and the multistep predicted *Dst* predicted by the *O'Brien and McPherron* [2000a] (OM) model and our model, respectively. Here all the data are hourly values.

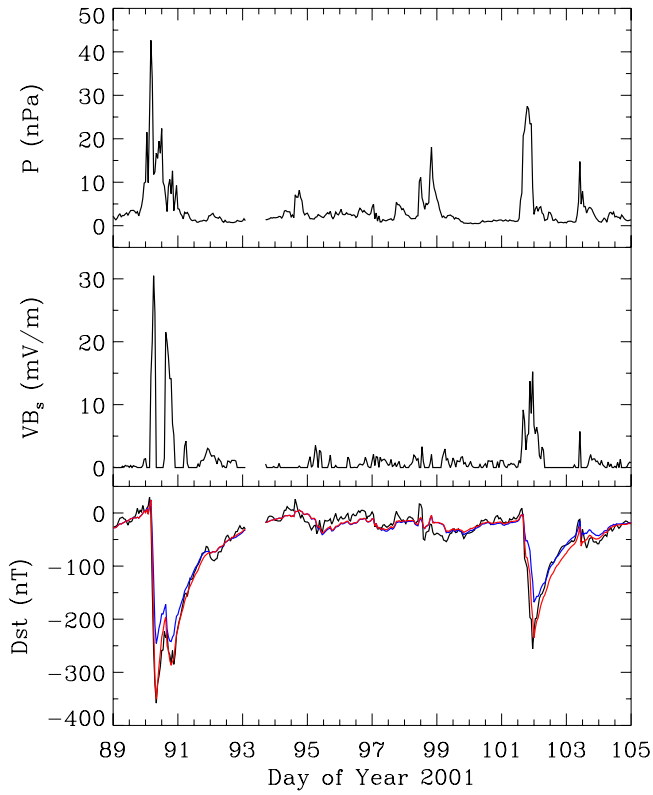


**Figure 6.** Solar wind and *Dst* parameters for two intense storms during the period from 30 March to 15 April 2001 with the same format as in Figure 5.

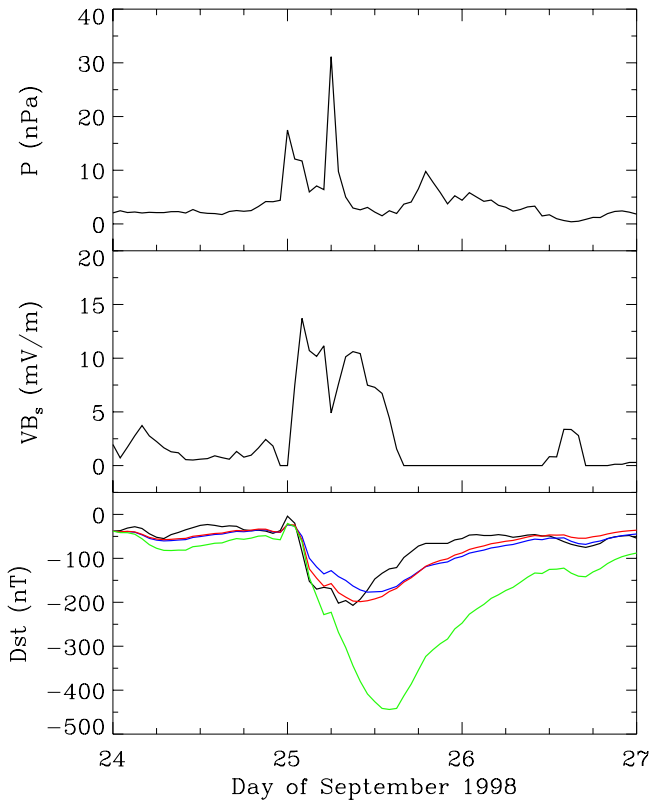


**Figure 7.** Solar wind and *Dst* parameters for the 24–27 September 1998 storm with the same format as in Figure 5. (bottom) Black, blue, red, and green curves representing the measured *Dst* and the multistep predicted *Dst* predicted by the OM model, our model, and the *Burton et al.* [1975] (B75) algorithm, respectively. When using higher resolution data, the B75 model also overestimates the minimum measured *Dst* value as shown in Figure 4 of *Liemohn and Ridley* [2002].